

1
2
3
4
5
6
7
8
9
10
11
12
13
14
15
16

Distinct effects of Fine and Coarse Aerosols on Microphysical Processes of Shallow
Precipitation Systems in Summer over Southern China

Fengjiao Chen^{1,2}, YuanjianYang^{3*}, Lu Yu¹, Yang Li¹, Weiguang Liu¹, Yan Liu^{1,4},
Simone Lolli⁵

¹ Key Laboratory of Transportation Meteorology of China Meteorological Administration, Nanjing
Joint Institute for Atmospheric Sciences, Nanjing, China

² China Meteorological Administration Radar Meteorology Key Laboratory, Beijing, China

³ School of Atmospheric Physics, Nanjing University of Information Science and Technology,
Nanjing, Jiangsu, China

⁴ State Key Laboratory of Severe Weather, Chinese Academy of Meteorological Sciences, Beijing,
China.

⁵ CNR-IMAA, Contrada S. Loja, 85050 Tito Scalo (PZ), Italy

*Corresponding author: Prof. Yuanjian Yang (yyj1985@nuist.edu.cn)

17 **Abstract:** The densely populated South China, adjacent to the South China Sea, which
18 is associated with shallow precipitation during summer, is an open-air natural
19 laboratory for studying the impact of aerosols on shallow precipitation events. Using
20 eight years of GPM DPR, MERRA-2 aerosol and ERA reanalysis data, this study
21 investigates the potential influence of coarse and fine aerosol modes on the structure of
22 the precipitation and the microphysical processes of shallow precipitation in South
23 China. Statistical results indicate that during coarse aerosol-polluted conditions,
24 shallow precipitation clouds have a lower mean height of the storm top (STH, ~ 3.2 km),
25 but a higher mean near-surface rainfall (RR, ~ 1.78 mm h⁻¹), characterized by high
26 concentrations of large raindrops, driven mainly by significant collision-coalescence
27 processes (accounting for 74.1%). In contrast, during fine aerosol-polluted conditions,
28 shallow precipitation clouds develop a deeper median STH ~ 3.7 km with lower surface
29 RR characterized by a low concentration of small hydrometeors, resulting from
30 increased breakup processes (33.1%) and reduced collision-coalescence processes
31 (69.6%). The coarse (fine) aerosols act as promoters (inhibitors) of radar reflectivity in
32 the profile of shallow precipitation, regardless of dynamic and humid conditions. The
33 effect of coarse aerosols in promoting precipitation and the inhibiting effect of fine
34 aerosols are the most significant under low humidity conditions, mainly attributed to
35 significantly enhanced collision-coalescence processes, exceeding 22.2%. Furthermore,
36 the increase in RR above 3 km during coarse aerosol-polluted environments is mainly
37 driven by the high concentration of hydrometeors in low instability conditions, whereas
38 by large hydrometeors in high instability environments.
39

40 **Short Summary:** The microphysical mechanisms of precipitation responsible for the
41 varied impacts of aerosols on shallow precipitation remain unclear. This study reveals
42 that coarse aerosols invigorate shallow rainfall through enhanced coalescence processes,
43 whereas fine aerosols suppress shallow rainfall through intensified microphysical
44 breaks. These impacts are independent of thermodynamic environments, but are more
45 significant in low-humidity conditions.
46

47 *1 Introduction*

48 Shallow precipitation, generally identified by storm height, dominates in marine
49 regions such as the ocean and marine continent, potentially accounting for 20% of
50 rainfall over tropical oceans and 7.5% over tropical land (Liu and Zipser, 2009; Chen
51 et al., 2016; Short and Nakamura, 2000). This underscores its crucial significance in the
52 regulation of the global water cycle. However, shallow precipitation is a complex
53 phenomenon influenced by various factors such as water vapor, thermodynamic
54 environment, and aerosols (Lang et al., 2021; Chen et al., 2024; Smalley and Rapp,
55 2020). Aerosols, as one of these factors, have sparked significant debate due to the
56 intricate nature of aerosol-radiation and aerosol-cloud interactions among various
57 species, resulting in unanswered questions about whether aerosols will increase or
58 decrease shallow precipitation (Koren et al., 2014; Fan et al., 2020; Christensen and
59 Stephens, 2012).

60 The impact of aerosols on precipitation has been widely investigated in many
61 previous studies (Sun and Zhao, 2021; Miltenberger et al., 2018; Liu et al., 2022; Fan
62 et al., 2018). Regional differences show that aerosols can delay the start time of
63 precipitation by 2 hours in the Pearl River Delta but advance by 3 hours in the North
64 China Plain (Sun and Zhao, 2021). Furthermore, precipitation is suppressed for
65 stratocumulus and small cumulus clouds in highly polluted environments, but enhanced
66 for heavy precipitation events and deep convective clouds (Yuan et al., 2011; Rosenfeld
67 et al., 2008; Xiao et al., 2022; Miltenberger et al., 2018). However, convective rainfall
68 invigoration depends on aerosol concentrations, which turns into suppression at the
69 turning zone of aerosol optical depth in 0.25-0.30 (Guo et al., 2019), potentially linked

70 to a change from aerosol microphysical effects to aerosol radiative effects (Jiang et al.,
71 2016). Liu et al. (2022) examined various aerosol types and discovered that marine
72 warm clouds experienced a fourfold increase in rainfall flux in the presence of high
73 levels of coarse spray aerosols, while there was a reduction by 75% in conditions with
74 high concentrations of fine aerosols. Additionally, these contrast effects are independent
75 of meteorological conditions. Another study suggests that the improvement of rainfall
76 in orographic regions with high mineral dust concentrations is more significant in
77 humid environments (Zhang et al., 2020b). Overall, the effects of aerosols on
78 precipitation depend on numerous elements such as weather conditions, types of
79 aerosols, their concentration, types of clouds, among others, and thus need to be
80 carefully analyzed.

81 Most of these studies on the interactions between aerosols and precipitation have
82 focused on the intensity, frequency of precipitation, and start and peak times of
83 precipitation, but few studies have reported on how aerosols impact rainfall through
84 modulating microphysical structures and processes of precipitation. Using three-
85 dimensional observations of precipitation and microphysics from dual frequency
86 precipitation radar (DPR) onboard the Global Precipitation Mission (GPM), recent
87 studies have revealed that aerosol mainly reduces mean droplet concentration and
88 increases the effective radius of precipitation in most regions of eastern China (except
89 Northeast China) (Sun et al., 2022); Xiao et al. (2022) found that the aerosol
90 invigoration effect on convective rainfall is characterized by higher droplet
91 concentration with smaller size under polluted conditions in Northeast China. However,
92 the impact of different aerosol species on precipitation microphysical structures and
93 microphysical processes (i.e., coalescence efficiency of rain droplets) has been scarcely
94 examined, which is essential for comprehending the full picture of the connections
95 between aerosols, precipitation microphysics, and precipitation.

96 South China (18~29°N, 110~123°E) is a region where shallow precipitation occurs
97 frequently (occurrence frequency up to 20%), and different types of aerosols prevail
98 during summer (Yang et al., 2021), making it an ideal region for the study of the aerosol
99 effect on shallow precipitation. Using the combined data set of GPM DPR and

100 MERRA-2 (Modern-Era retrospective analysis for Research and Applications,
101 Versions2), this study aims to answer the following questions: 1) Do coarse and fine
102 aerosols enhance or diminish the surface precipitation associated with shallow
103 precipitation? 2) In what manner do aerosols influence the microphysical structures or
104 processes of precipitation (such as break-up and collision-coalescence)? 3) To what
105 extent are the relationships between aerosols and rainfall, microphysical structures, and
106 processes sensitive to the dynamical and vapor components? The data and methods are
107 introduced in Section 2. Section 3 discusses the impacts of fine and coarse aerosols on
108 the microphysical properties and processes for shallow precipitation. A summary and
109 conclusions are presented in Section 4.

110

111 ***2 Data and Methods***

112 ***2.1 Data***

113 In this study, four different data set are used to illustrate the potential impact of
114 aerosols on microphysical precipitation structures and shallow precipitation processes
115 over southern China during the summers between 2014 and 2021.

116 In the present study, the hourly MERRA-2 aerosol dataset
117 (MERRA2_400.tavg1_2d_aer_Nx) at 0.5×0.625 spatial resolution is used, which has
118 been widely utilized with the advantage of high temporal and spatial resolution.
119 MERRA-2 is produced using the Goddard Earth Observing System, Version 5 (GEOS-
120 5) atmospheric model and the Gridpoint Statistical Interpolation (GSI) assimilation
121 system (Molod et al., 2015). GEOS-5 integrates a radiatively coupled version of the
122 Goddard Chemical Aerosol Radiation and Transport (GOCART) model to simulate
123 aerosol components (Chin et al., 2002). In the estimation of aerosol properties,
124 MERRA-2 assimilates aerosol data from ground-based observations from Aerosol
125 Robotic NETWORK (AERONET) and spaceborne aerosol products from Advanced Very
126 High Resolution Radiometer (AVHRR), Multiangle Imaging Spectro Radiometer

127 (MISR) (Randles et al., 2017; Buchard et al., 2017). Previous studies have shown a
128 relatively good consistency of AOD from MERRA-2 and ground-based observations,
129 i.e., AERONET, Sun sky radiometer Observation NETwork (SONET) (Ou et al., 2022;
130 Buchard et al., 2015; Sun et al., 2019a). The correlation coefficient between MERRA-
131 2 AOD and AERONET could reach 0.92 in summer China (Sun et al., 2019a). However,
132 there is a slight underestimation of MERRA-2 AOD when compared to situ
133 observations. Ou et al. (2022) revealed that the MERRA-2 AOD is underestimated by
134 approximately 0.1 compared to a SONET station over South China. This is mainly
135 because MERRA-2 lacks nitrate aerosols, leading to underestimations in the estimation
136 of total AOD and fine aerosols (Sun et al., 2019b; Ou et al., 2022). The fine and coarse
137 aerosol environment is defined by not only the AOD thresholds but also the AOD
138 fractions to the total AOD, which may reduce uncertainties caused by underestimating
139 AOD to some extent.

140 Aerosol species, including black carbon, organic carbon, sulfate, sea salt, and dust,
141 are assumed to be external mixtures that do not interact with each other. In this present
142 study, we consider the aerosol optical thickness and the extinction at 550 nm for five
143 species, i.e. black carbon, organic carbon, sulfate, sea salt, and dust, as well as the
144 Angstrom exponent (α) between 470 and 870 nm. α is a significant parameter in aerosol
145 science, which elucidates the AOD dependency on wavelength. A higher α is related to
146 a higher concentration of fine particles, whereas a lower α suggests a higher
147 concentration of coarse particles (Lolli et al., 2023).

148 The GPM DPR consists of two precipitation radars operating in the Ka and Ku
149 bands, providing a unique opportunity to obtain information on three-dimensional
150 precipitation and particle drop size distributions (DSDs) at the same time. In the present
151 study, the official 2ADPR (version 7) dataset covering the summers (June to August)
152 of 2014 and 2021 is also used, which provides information on the observation time,
153 near-surface rain rate (RR), liquid water path (LWP), the three-dimensional profiles of
154 attenuation-corrected reflectivity (Z_e), rainfall, the mass-weighted mean diameter D_m
155 (in mm) and the generalized intercept N_w (in $\text{mm}^{-1} \text{m}^{-3}$) of the normalized gamma
156 distributions with a vertical resolution of 125 m in each scanning pixel (Iguchi et al.,

157 2017). The reliability of DSDs and precipitation has been validated by many previous
158 studies (Huang et al., 2021; Radhakrishna et al., 2016). Due to the high spatial
159 resolution (125m in vertically and 4.5 km in horizontal resolution), the official 2ADPR
160 (version 7) dataset has been widely used in the field of climatology (Chen et al., 2024;
161 Zhang et al., 2020a; Chen et al., 2020). Shallow precipitation clouds are defined by
162 their near-surface RR exceeding 0.1 mm h^{-1} and STH below 5 km in altitude. The storm
163 top height (STH) is defined as the maximum height where the Z_e exceeds 20dBZ (Liu
164 and Zipser, 2013).

165 In this study, convective available potential energy (CAPE) and relative humidity
166 (RH) at 850 hPa from the fifth-generation global reanalysis of the European Center for
167 Medium-Range Weather Forecasts (ERA5) covering the period from 2014 to 2021 are
168 also used to investigate the meteorological dependence on the relationship between
169 aerosols and precipitation. Additionally, the global 1km grid quality-controlled global
170 digital elevation model (DEM) (<https://ngdc.noaa.gov/mgg/topo/globe.html>) is also
171 used to exclude the influence of topography in the present study.

172

173 **2.2 Methods**

174 Due to the different spatial and temporal resolutions of DPR, MERRA-2, and
175 ERA5, Prior to examining the potential influence of various aerosol types on shallow
176 precipitation, it is necessary to harmonize these three datasets. Since the DPR detects
177 the rainy pixels at approximately 4.5 km spatial resolution, both MERRA-2 at $0.5 \times$
178 0.625° resolution and ERA5 at 0.25° resolution are first linearly interpolated to 0.05°
179 resolution. To accurately depict the aerosol conditions preceding shallow precipitation,
180 observations of AOD from MERRA-2, corresponding closely to the timing of DPR
181 observations and with a spatial resolution of 0.05° , are utilized. Concurrently,
182 atmospheric data derived from ERA5 at a 0.05° resolution, which is in closest proximity
183 to the center and observation time of the DPR pixel, are also used. The aerosol fine
184 mode AOD is defined as the total AOD sum of partial AOD of black carbon, organic

185 carbon, and sulfate, while the AOD of coarse aerosols is the total value of the sum of
186 AOD values of sea salt and dust particles (Gelaro et al., 2017). Additionally, to
187 eliminate the potential impact of topography on precipitation and aerosol analysis, the
188 study includes only shallow precipitation pixels that occur over regions with a
189 topographic elevation of less than 100 meters.

190

191 Figure 1a illustrates the probability density of the joint distribution of AOD and α
192 prior to the occurrence of the shallow precipitation event. Shallow precipitation is most
193 probable when the AOD is approximately 0.4 and α is approximately 1.4, which
194 suggests a predominance of the fine aerosol mode. This can be primarily attributed to
195 the increased presence of fine aerosols in South China during summer season, as
196 represented in Figure 1b, where the probability density distributions (PDF) of AOD for
197 fine aerosols and total aerosols reveal comparable values. Nonetheless, shallow
198 precipitation is also evident in settings characterized by coarse aerosols, exhibiting a
199 significant frequency when α is less than 1 and AOD is less than 0.3, as shown in Figure
200 1a.

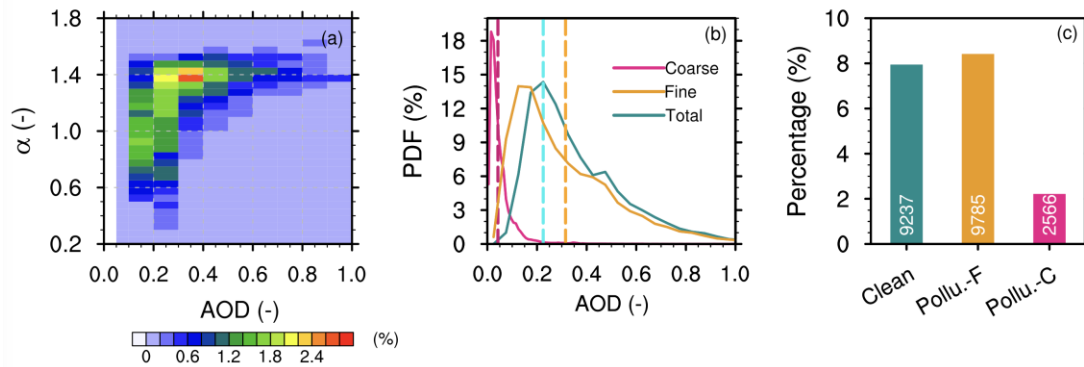
201 There are three types of aerosol conditions discussed in the present study: clean
202 environment, fine aerosol-polluted environment, and coarse aerosol-polluted
203 environment. To classify clean and aerosol-polluted conditions over South China, PDFs
204 of AOD for fine, coarse, and total aerosols are calculated before shallow precipitation,
205 as shown in Figure 1b. It can be observed that the coarse mode AOD is relatively small,
206 primarily distributed between 0 and 0.2, while fine mode AOD and total AOD are
207 almost equal, mainly concentrated between 0 and 1.0. Specifically, the peak frequency
208 occurs at an AOD of approximately 0.1 for coarse aerosols, 0.15 for fine aerosols, and
209 0.2 for total aerosols. We define a clean environment as one in which the AOD of the
210 total aerosols falls below the 30th percentile in all the data sampled, specifically the
211 AOD of the total aerosols < 0.225 (see Table 1 for reference). A fine (or coarse) aerosol-
212 polluted environment must not only exceed 60% quantiles across all sampled data but
213 also have the AOD of fine (or coarse) particles exceeding 50% of the total aerosol AOD.
214 This approach ensures that in fine (or coarse) aerosol-polluted environments, fine (or

215 coarse) particles are the primary influencing factor. Based on these standards, a coarse
216 aerosol-polluted environment is classified as having a coarse AOD > 0.0425 , as well as
217 the proportion of coarse AOD to total aerosols exceeds 50%. Similarly, a fine aerosol-
218 polluted environment is defined by a fine AOD > 0.315 , with the proportion of fine
219 AOD to total aerosols exceeding 50% (see Table 1 for reference). A sensitivity test was
220 conducted with different thresholds to ensure the robustness of the present study. The
221 results indicate that varying the thresholds does not significantly affect the conclusions
222 of the work. During the study period, there are 9237, 9785, and 2566 shallow
223 precipitation samples under clean, fine aerosol, and coarse aerosol-polluted conditions,
224 respectively (Figure 1c). The mean AODs of five aerosol species under various
225 environmental conditions are calculated to understand the contributions of different
226 aerosol types (not shown). In South China, the primary contributors to aerosol species
227 are sulfate aerosol, sulfate aerosol, and sea salt aerosols in clean, fine, and coarse
228 aerosol-polluted environments, respectively. The shallow precipitation accounts for a
229 higher proportion with respect to the total precipitation samples, reaching $\sim 8\%$ in clean
230 and fine aerosol-polluted conditions (Figure 1c). However, under coarse aerosol-
231 polluted conditions, the proportion of shallow precipitation samples is much lower, at
232 around $\sim 2\%$. Due to the lower AOD of coarse aerosol mode, occurrences, where the
233 AOD of coarse aerosols accounts for more than 50% of the total AOD are less frequent,
234 which explains the lower shallow precipitation samples in coarse aerosol-polluted
235 conditions. However, the approximately 2500 samples ensure the reliability of our
236 research results to some extent.

237

238

239



240

241

242

243

244

245

246

247

248

249

250

251

252

Figure 1 The observed frequency of AOD and α prior to the occurrence of shallow precipitation is illustrated in (a). The probability distribution functions of AOD for fine, coarse, and total aerosols before the shallow precipitation event are depicted in (b). The proportion of shallow precipitation samples relative to total precipitation samples, categorized by different aerosol conditions, is shown in (c), as recorded by DPR in southern China during the summers from 2014 to 2021. The pink vertical line (orange) in (b) represents the upper 60% threshold for fine (coarse) aerosols, respectively. The cyan vertical line in (b) denotes the lower 30% threshold for the total AOD. The shallow precipitation samples are represented by white text in (c).

Table 1 Definitions of polluted and clean conditions of coarse and fine aerosol modes in southern China during the summers from 2014 to 2021.

Environment	Definition
Clean	Total AOD < 0.225
Polluted_Fine	Fine AOD > 0.315 & Fine AOD ratio > 50%
Polluted_Coarse	Coarse AOD > 0.0425 & Coarse AOD ratio > 50%

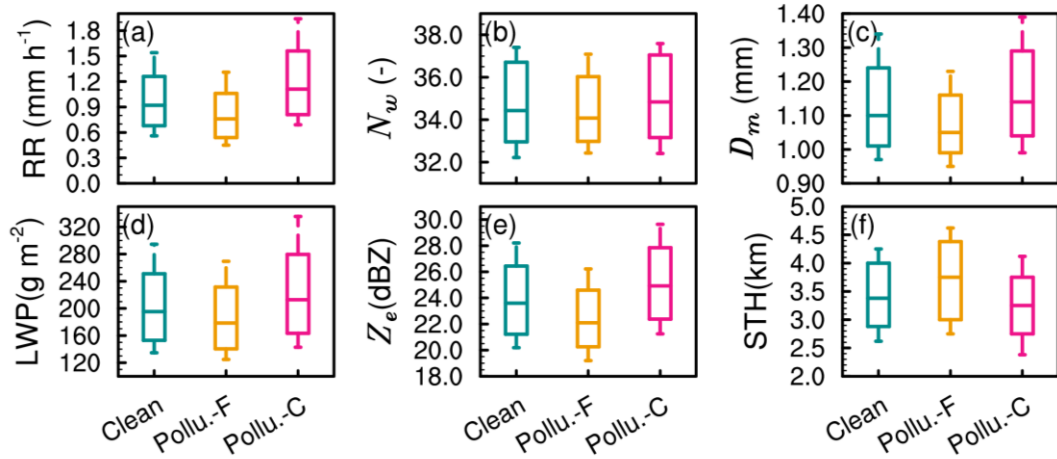
253

254 **3 Results**

255 **3.1 Influence of aerosol on rainfall and microphysical characteristics**

256 Figure 2 exhibits boxplots illustrating the near-surface RR, N_w , D_m , and Z_e at an

257 altitude of 2.5 km, alongside LWP and STH, for shallow precipitation under varying
258 aerosol conditions in South China. Compared to clean environment, the RR decreases
259 slightly during fine mode aerosol pollution conditions, with a median value of only 0.7
260 mm h⁻¹, while in presence of coarse mode aerosol-polluted environment, the median
261 value of RR increases, reaching 1.0 mm h⁻¹. This is consistent with a higher median Z_e
262 at 2.5 km in altitude (25 dBZ) under coarse aerosol-polluted conditions and a lower one
263 (22 dBZ) under fine aerosol-polluted conditions, suggesting the inhibition effect of fine
264 particles and the invigoration effect of coarse particles on the near-surface RR for
265 shallow precipitation. Nevertheless, the presence of coarse aerosol-polluted conditions
266 appears to inhibit the vertical development of shallow precipitation clouds (Figure 2f),
267 with a significantly lower median STH (~3.2 km) than that (~3.7 km) for fine aerosol-
268 polluted environments. Examining the situation from a microphysical standpoint, it is
269 observed that in comparison to a clean environment, there is a reduction in the median
270 values of LWP at approximately 170 g m⁻², number concentration of droplets (N_w) at
271 34, and mass-weighted mean diameter (D_m) at 1.05 mm at an altitude of 2.5 km in fine
272 mode aerosol environments. On the contrary, under coarse aerosol-polluted conditions,
273 the median values of LWP, N_w , and D_m at 2.5 km altitude increase, reaching 210 g m⁻²,
274 35, and 1.15 mm, respectively. This indicates that the enhancement of near-surface RR
275 under coarse aerosol-polluted conditions is contributed by higher concentrations of
276 large rain droplets, while the weakening under fine aerosol-polluted conditions is
277 influenced by lower concentrations of small rain droplets. In South China, sea salt
278 aerosols are the primary components of coarse particles, and a recent study by Liu et al.
279 (2022) has shown that sea salt aerosols are more likely to form large cloud droplets
280 through hygroscopic growth, which are more likely to form rain droplets through
281 condensation and other microphysical processes, resulting in higher cloud water
282 content within shallow precipitation clouds. On the contrary, fine aerosols tend to
283 reduce the effective radius of cloud droplets, with small cloud droplets being prone to
284 evaporation and subsequent loss of cloud water. Our results fill the gap between cloud
285 microphysics, precipitation microphysics, and precipitation.



286

287

288

289

290

291

292

293

294

295

296

297

298

299

300

301

302

303

304

305

306

307

308

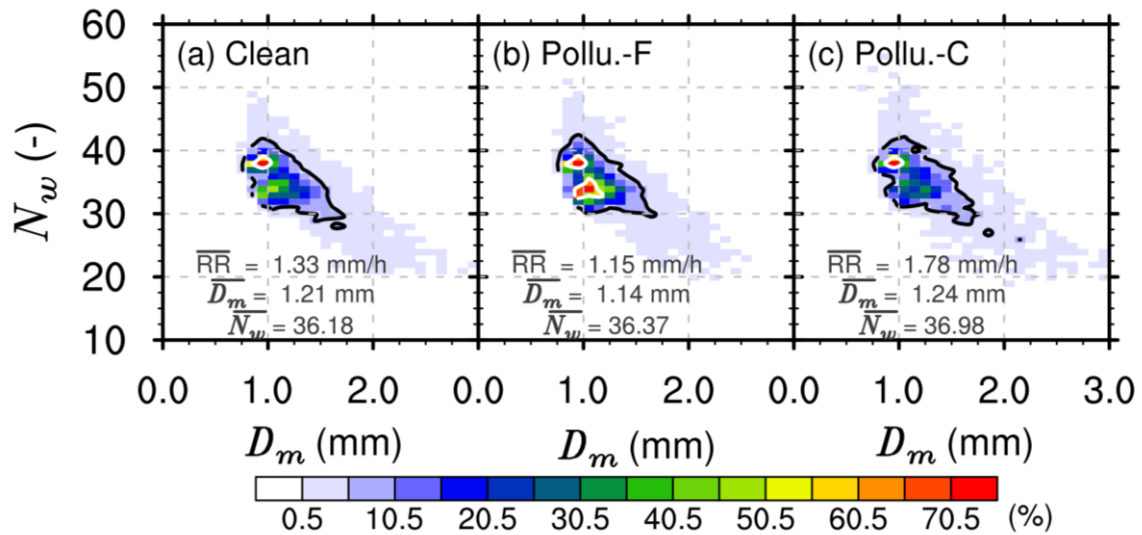
Figure 2 The box plot presents the near-surface rain rate (a), N_w (b), D_m (c), LWP (d), Z_e (e), and STH (f) for shallow precipitation across varying aerosol conditions in southern China during the summer seasons from 2014 to 2021. The top and bottom edges of the boxes indicate the upper and lower tritile, respectively. The line inside the box denotes the median. The whiskers extending from the box illustrate the upper and lower quartiles.

DSDs directly impact RR. Therefore, the DSDs at 2.5 km altitude for shallow precipitation clouds over southern China under three aerosol conditions are illustrated in Figure 3. Irrespective of the aerosol background, the DSDs are characterized by a high concentration of small particles and a low concentration of large particles, aligning with prior research findings (Wang et al., 2016; Chen et al., 2022). In a clean environment (Figure 3a), the DSD of shallow precipitation exhibits a high-frequency center around N_w of approximately 40, with D_m around 1.0 mm, reaching a frequency exceeding 70%. A secondary peak (40%) slightly shifts towards the lower right, located at D_m around 1.2 mm and N_w around 32. In the case of fine aerosol-polluted environments (Figure 3b), the average RR (1.15 mm h⁻¹) and D_m (1.14 mm) are slightly reduced compared to the clean environment, while the mean N_w increases slightly to 36.37. Furthermore, the secondary peak observed in a clean environment becomes more pronounced under fine aerosol-polluted conditions, with a frequency exceeding 50%. In contrast to clean and fine aerosol-polluted environments, both the mean values of RR and N_w increase under coarse aerosol-polluted conditions (Figure 3c). Furthermore,

309 the DSD reveals more samples with D_m exceeding 2 mm or N_w exceeding 40, further
 310 indicating the enhancement of RR for shallow precipitation in coarse aerosol-polluted
 311 environments.

312

313



314

315 **Figure 3** DSDs at 2.5 km altitude for shallow precipitation in clean (a), fine (b) aerosol-
 316 polluted and coarse (c) aerosol-polluted environments over southern China during the
 317 summers from 2014 to 2021. The mean values of D_m and N_w under different aerosol
 318 conditions are presented in each panel. The 5% and 50% contours are indicated by black
 319 and white solid lines, respectively.

320

321 *3.2 Influence of aerosol on microphysical structures and processes*

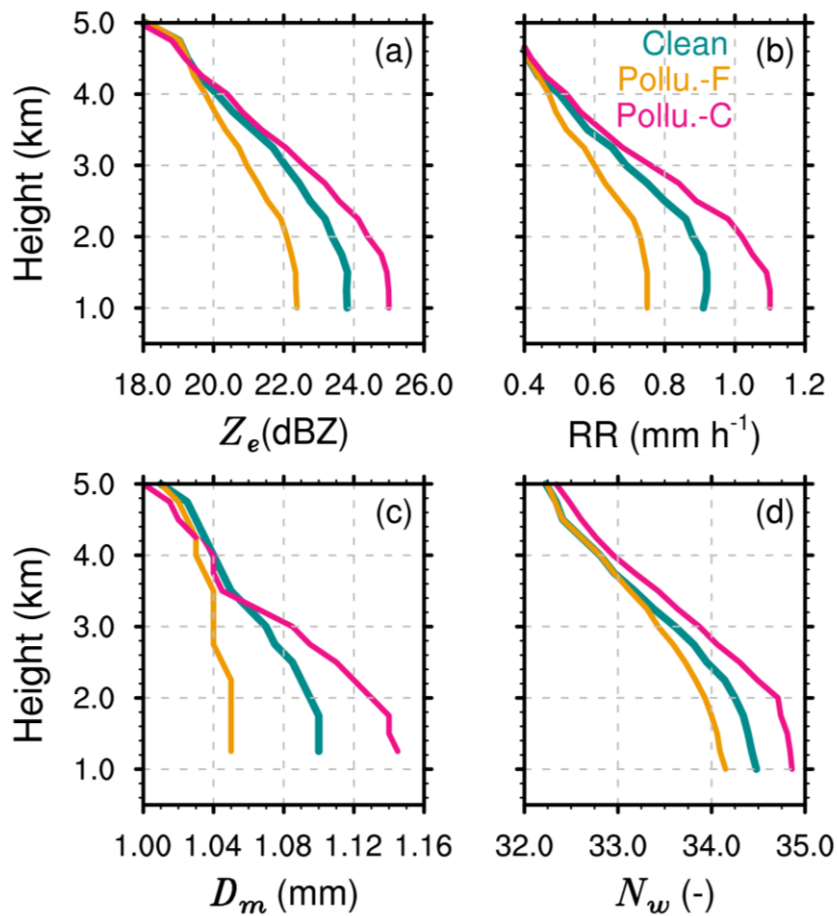
322 The above analysis has shown significant differences in near-surface RR and DSD
 323 for shallow precipitation under different aerosol environments. The vertical structure of
 324 precipitating clouds is closely related to near-surface RR and DSD, reflecting the
 325 thermal and dynamic structure within the clouds. Investigating the precipitation and
 326 microphysical structures under different aerosol backgrounds can further deepen our
 327 understanding of the thermodynamic and microphysical mechanisms by which aerosols
 328 affect shallow precipitation near the surface.

329 Figure 4 presents the profiles of the median values of Z_e , RR, D_m , and N_w for
330 shallow precipitation over southern China in summer in three different aerosol
331 environments. In general, shallow precipitation exhibits an increase in Z_e , RR, D_m , and
332 N_w with a decrease in altitude across various aerosol environments, suggesting that the
333 growth process of shallow precipitation is predominantly governed by warm rain
334 collision-coalescence mechanisms. This is similar to the precipitation structures for
335 shallow precipitation in the Yangtze-Huaihe River Basin (Chen et al., 2024). However,
336 the median values of Z_e , RR, D_m , and N_w at each altitude differ under different aerosol
337 environments. The promotion effect of coarse aerosols and the inhibition effect of fine
338 aerosols are present throughout the profile. For example, the median values of Z_e , RR,
339 D_m , and N_w at any given altitude are the largest in a coarse aerosol-polluted environment
340 and the smallest in a fine aerosol-polluted pollution. Furthermore, the most significant
341 differences in precipitation microphysical structures under different aerosol
342 backgrounds occur near the surface (below 2 km). For example, at 1 km altitude, the
343 differences in Z_e , RR, D_m , and N_w are approximately 3 dBZ, 0.4 mm h⁻¹, 0.12 mm and
344 1, respectively.

345 Considering the increasing amplitude of the median values of Z_e , RR, D_m , and N_w
346 with decreasing altitude, there are significant differences under different aerosol
347 backgrounds, reflecting different microphysical precipitation processes within shallow
348 precipitation systems. Specifically, in coarse aerosol-polluted environments, the
349 increases in Z_e , RR, D_m , and N_w within the same altitude layer are the largest, while the
350 increases in these variables are the smallest in fine aerosol-polluted environments. This
351 explains why a concentration increase of coarse particles results in an enhancement of
352 RR compared to a clean environment, whereas an increase in fine aerosols leads to a
353 precipitation suppression. For instance, the median D_m in pristine environments shows
354 an increment from 1.07 mm at 3 km altitude to 1.1 mm at 1 km. In environments
355 polluted by coarse aerosols, D_m exhibits a more pronounced increasing trend, with the
356 median D_m rising from 1.08 mm at 3 km to 1.14 mm at 1 km. Conversely, with fine
357 mode aerosols, the change in the median D_m from 3 km to 1 km is negligible, almost
358 remaining constant at approximately 1.04 mm.

359

360



361

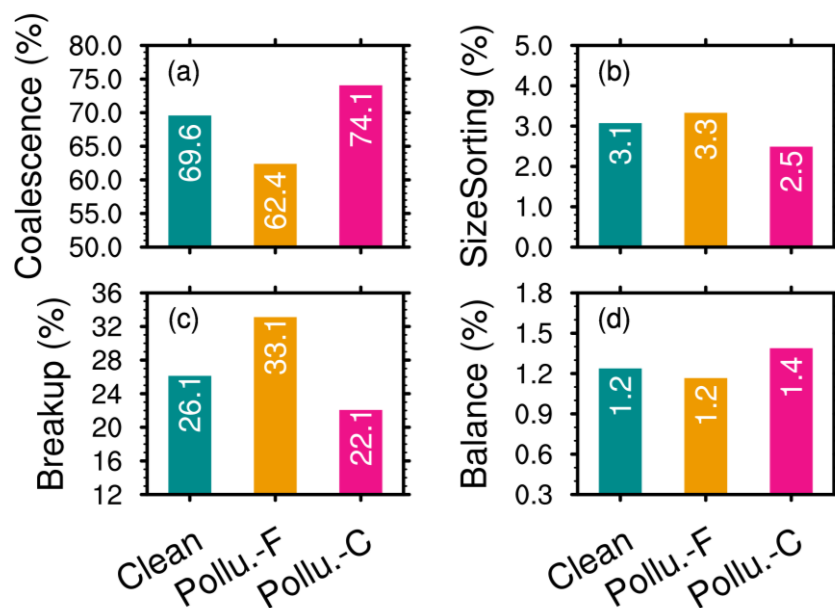
362 **Figure 4** The profiles of the median Z_e (a), rain rate (b), D_m (c), and N_w (d) for
363 shallow precipitation in different aerosol conditions over southern China during the
364 summers from 2014 to 2021.

365

366 To more intuitively reflect the potential impact of different aerosol types on the
367 near-surface microphysical processes of shallow precipitation, the methods of Kumjian
368 et al. (2014) are adopted to quantify the near-surface microphysical processes using
369 changes in Z_e ($\Delta Z_e = Z_e^{1\text{km}} - Z_e^{3\text{km}}$) and D_m ($\Delta D_m = D_m^{1\text{km}} - D_m^{3\text{km}}$) at 3 km and 1 km. For
370 example, collision-coalescence typically causes increases in Z_e and D_m , while breakup
371 causes decreases. Similarly, an upward trend in D_m combined with a downward trend
372 in Z_e as they approach the ground (positive ΔD_m and negative ΔZ_e) indicates
373 evaporation or size sorting is the dominant process. The signature of a "balance"

374 between collision-coalescence and breakup is shown by a minor reduction in D_m and a
375 rise in Z_e .

376 Figure 5 shows the proportions of collision-coalescence, size sorting, breakup, and
377 balance processes of raindrop particles in shallow precipitation clouds under three
378 different aerosol backgrounds. In general, the microphysical process of collision-
379 coalescence of hydrometeors dominates shallow precipitation, accounting for more
380 than 60%. This is followed by the hydrometeor breakup process, which accounts for
381 more than 20%, while size sorting and balance processes account for the smallest
382 proportions, only about 3% and 1%, respectively. In presence of fine aerosol-mode, the
383 proportion of the collision-coalescence process is only 62.4%, while this proportion
384 reaches 74.1% in coarse aerosol-polluted environments, with an increase of about
385 11.7%. Similarly, the proportion of the hydrometeor particle breakup process is 33.1%
386 (a decrease of 10%). This indicates the increase in the proportion of raindrop breakup
387 processes and the weakening of the collision-coalescence process in fine aerosol-
388 polluted environments, which may be the reason for the weakened near-surface RR.
389 Conversely, in coarse aerosol-polluted mode environments, raindrop hydrometeors
390 undergo more collision-coalescence growth processes and fewer breakup and
391 evaporation processes, which contributes to the enhancement of surface RR.



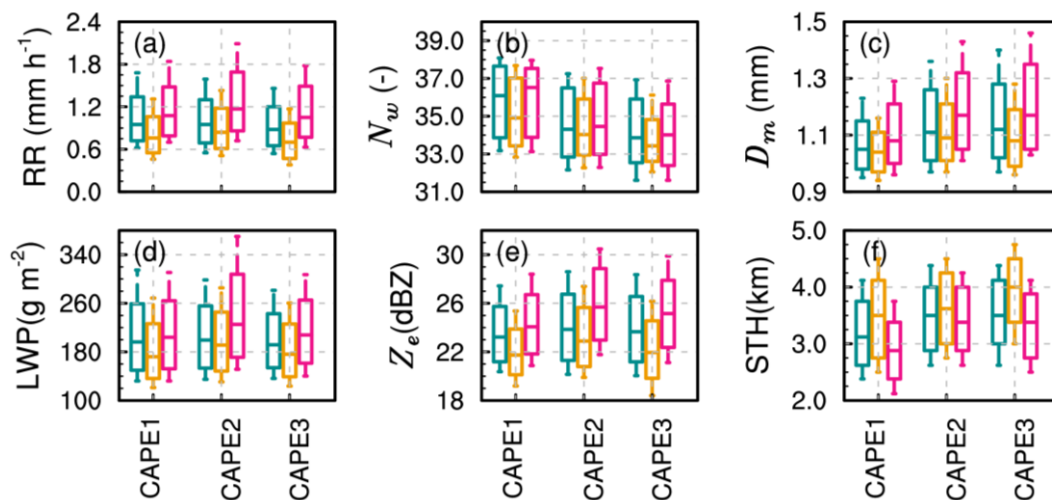
393 **Figure 5** The percentages of coalescence (a), size sorting (b), break up(c), and
394 balance (d) for shallow precipitation shallow precipitation rain hydrometeors under
395 different aerosol conditions in southern China during the summers from 2014 to 2021.
396

397 *3.3 Sensitivities of aerosol impacts on precipitation to meteorological factors*

398 The findings from the prior section demonstrate that shallow precipitation shows
399 notable variations in surface RR, precipitation structures, and microphysical processes
400 depending on different aerosol conditions. However, precipitation itself is a complex
401 process influenced by multiple thermal and dynamic environmental factors, such as
402 instability, humidity, temperature, and wind vectors. Among these, dynamic conditions
403 and moisture levels are particularly important indicators. Therefore, CAPE and RH at
404 850 hPa, which, respectively, reflect atmospheric instability and moisture, are used to
405 isolate and assess the impact of aerosols. CAPE is divided into three intervals based on
406 the terciles of CAPE values during precipitation events in southern China: CAPE 333
407 J kg^{-1} (CAPE1), $333 < \text{CAPE} < 1031 \text{ J kg}^{-1}$ (CAPE2), and CAPE 1031 J kg^{-1} (CAPE3).
408 Similarly, RH at 850 hPa is divided into three intervals, that is, RH 83% (RH1), $83\% <$
409 $\text{RH} < 91\%$ (RH2), and RH 91% (RH3).

410 The box plots of RR, LWP, and STH, as well as N_w , D_m , and Z_e at 2.5 km altitude
411 for shallow precipitation in southern China under different aerosol backgrounds and
412 CAPEs are presented in Figure 6. Consistent with the conclusions of Figure 2, it
413 becomes apparent that under varying CAPE conditions, the median STH of shallow
414 precipitation clouds attains its lowest values in coarse aerosol-polluted environments,
415 whereas the median RR and Z_e at an altitude of 2.5 km reach their highest levels. On
416 the contrary, the median STH is the highest, but the median RR and Z_e at 2.5 km are the
417 lowest in a fine aerosol-polluted environment. This indicates that the suppression of RR
418 in fine aerosol-polluted environments and the invigoration of RR in coarse aerosol-
419 polluted environments are independent of the dynamic conditions (CAPE in this case).
420 Furthermore, when seen from microphysics, under different CAPE conditions, shallow

421 precipitation clouds in coarse aerosol-polluted environments exhibit the highest median
 422 values of values of LWP, N_w , and D_m at 2.5 km, while these variables are the lowest in
 423 fine aerosol-polluted environments. This helps explain why shallow precipitation has
 424 the highest near-surface RR in coarse aerosol-polluted environments and the lowest
 425 surface RR in fine aerosol-polluted environments from the microphysical perspective.
 426



427

428 **Figure 6** Box plot of the near-surface rain rate (a), N_w (b), D_m (c), LWP (d), Z_e (e),
 429 and STH (f) under different aerosol and CAPE conditions for shallow precipitation over
 430 southern China during the summers of 2014-2021. The boxes' top and bottom edges
 431 indicate the upper and lower tritile, respectively. The median is depicted by the line
 432 inside the box. The whiskers extending from the box illustrate the lower and upper
 433 quartiles.

434

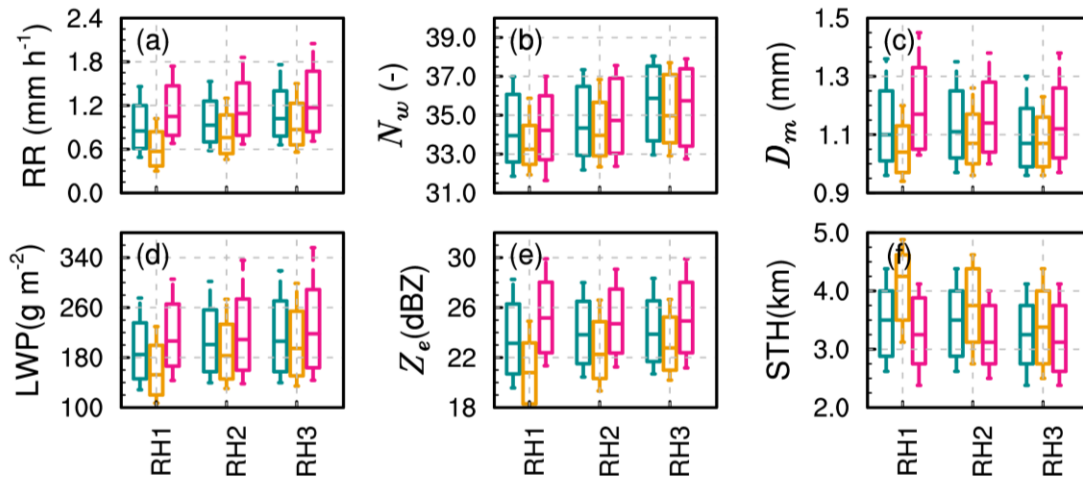
435 Similarly, the sensitivity of humidity to the impact of aerosol on shallow
 436 precipitation is examined by presenting the box plots of precipitation parameters, as
 437 illustrated in Figure 7. Regardless of 850hPa-RH, the vertical development of shallow
 438 precipitation clouds is hindered in coarse aerosol-polluted environments, with the
 439 median STH being the smallest. However, the near-surface RR is the highest,
 440 corresponding to the highest median Z_e at 2.5 km. On the contrary, in fine particle
 441 pollution environments, the vertical development of shallow precipitation clouds is

442 enhanced (with the highest median STH), but the near-surface RR and Z_e are the
443 weakest. This further confirms that the impact of coarse and fine aerosols on near-
444 surface RR and LWP is independent of moisture and dynamic conditions.

445 It is important to note that the degree of enhancement or suppression of RR by
446 coarse and fine aerosols varies under different humidity conditions. Compared to high-
447 humidity environments, coarse aerosols have the most significant enhancement effect
448 on RR, while fine aerosols have the most significant suppression effect in relatively
449 low-humidity environments (RH1). In fine aerosol-polluted environments, the box plot
450 of RR shows a significant decrease compared to that in clean environments, while that
451 in coarse aerosol-polluted environments shows a significant increase. Specifically, the
452 median RR in the coarse aerosol-polluted environment is around 1.1 mm h^{-1} , while it is
453 around 0.7 mm h^{-1} in the fine aerosol-polluted environment.

454 Regarding STH, under low relative humidity and fine aerosol pollution conditions,
455 shallow precipitation clouds develop more deeply, with the 25th percentile of STH
456 reaching 5 km, significantly higher than in clean and coarse aerosol-polluted
457 environments. This may be because there is a reduction in the effective radius of cloud
458 droplets in fine aerosol-polluted and low-humidity conditions. Smaller cloud droplets
459 are more prone to evaporation, resulting in a lower LWP, which does not favor an
460 increase in near-surface RR. This is also reflected in the near-surface DSD, which is
461 characterized by lower N_w and smaller D_m . However, although the humidity is relatively
462 low, the coarse particles, being more hygroscopic, can form larger cloud droplets,
463 reducing the loss of cloud water due to evaporation (resulting in a higher LWP), and
464 thereby enhancing surface RR. This is also reflected in the near-surface DSD, which is
465 characterized by a higher N_w and larger D_m . In high humidity environments, a high
466 concentration of fine particles can promote the formation of more cloud condensation
467 nuclei, which to some extent reduces the loss of cloud water due to the evaporation of
468 small particles. Therefore, the LWP in fine-particle pollution environments does not
469 differ much from that in coarse aerosol-polluted environments. This may also lead to
470 smaller differences in RR, Z_e , and other variables between coarse and fine aerosol-
471 polluted environments under relatively high humidity conditions.

472



473

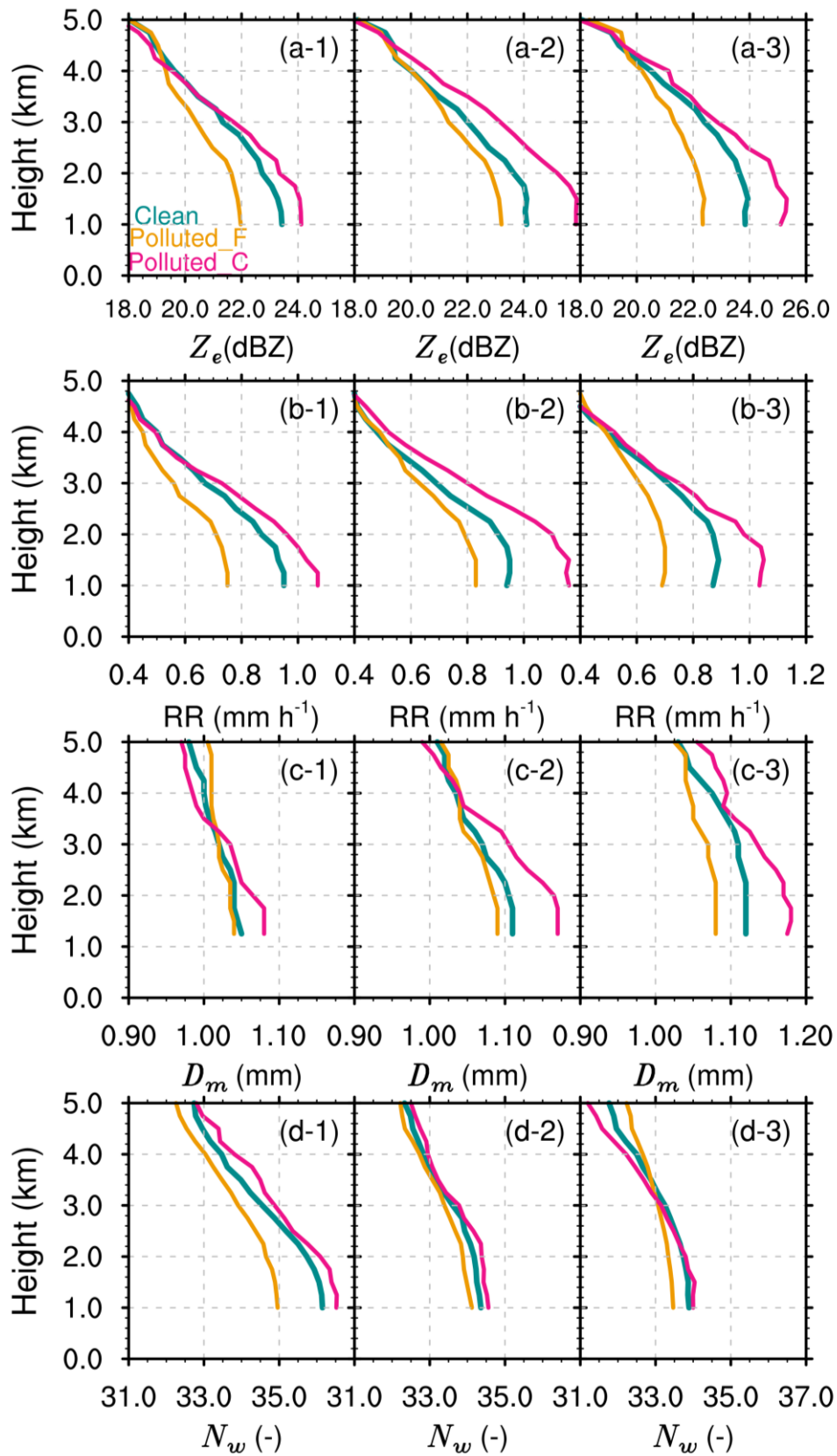
474 **Figure 7** Same as Figure 6, but for RH at 850hPa.

475

476 **3.4 Sensitivities of aerosol impacts on microphysical structures and processes to**
477 **meteorological factors**

478 This part continues examining how coarse and fine aerosol modes affect
479 precipitation structure and the microphysical processes in different environmental
480 settings. As shown in Figure 8, under different CAPE and aerosol backgrounds, shallow
481 precipitation profiles consistently exhibit increasing trends in Z_e, RR, N_w, and D_m with
482 decreasing altitude. Furthermore, irrespective of CAPE values, at a specified altitude,
483 the parameters Z_e and RR are observed to be at their maximum in aerosol coarse mode
484 environments polluted with coarse aerosols, followed by those in a clean environment,
485 and at their minimum in environments polluted with fine aerosols. This is consistent
486 with the results in Figure 4. When compared between different CAPE conditions, the
487 Z_e, RR, and D_m of shallow precipitation in CAPE2 are the highest at different altitudes,
488 while as the CAPE increases further (CAPE3), these values even decrease. Apart from
489 instability, precipitation can be influenced by moisture, topography, and other factors;
490 therefore, it is possible for an even lower RR in high CAPE conditions.

491 When seen from D_m and N_w (Figures 8c1-c3, d1-d3), the promotion effect of
492 coarse aerosols and the suppression effect of fine aerosols can vary under different
493 dynamic environmental conditions. Under moderate CAPE conditions (CAPE2), D_m
494 and N_w in coarse aerosol-polluted environments are the largest at different altitudes,
495 while D_m and N_w in a fine aerosol-polluted environment are the smallest. This indicates
496 that under moderate CAPE conditions, the enhancement of RR in coarse aerosol-
497 polluted environments is contributed by large particles and high concentrations. For
498 low CAPE conditions (CAPE1), the median D_m above 3 km is even the smallest in
499 coarse aerosol-polluted environments, compared to clean and fine aerosol-polluted
500 environments. Therefore, the maximum values of RR and Z_e at this layer are mainly
501 contributed by high concentrations of raindrop particles (with large median N_w , as
502 shown in Figure 8d-1). For high CAPE conditions (CAPE3), the median N_w above the
503 3 km altitude layer in coarse aerosol-polluted environments is even the smallest.
504 Therefore, the maximum values of RR and Z_e at this altitude are mainly contributed by
505 high concentrations of raindrop particles (with large median D_m , as shown in Figure 8c-
506 3).



507

508 **Figure 8** The Z_e (a), rain rate (b), D_m (c), and N_w (d) profiles for shallow precipitation
 509 in different aerosol and CAPE conditions over southern China during the summers from

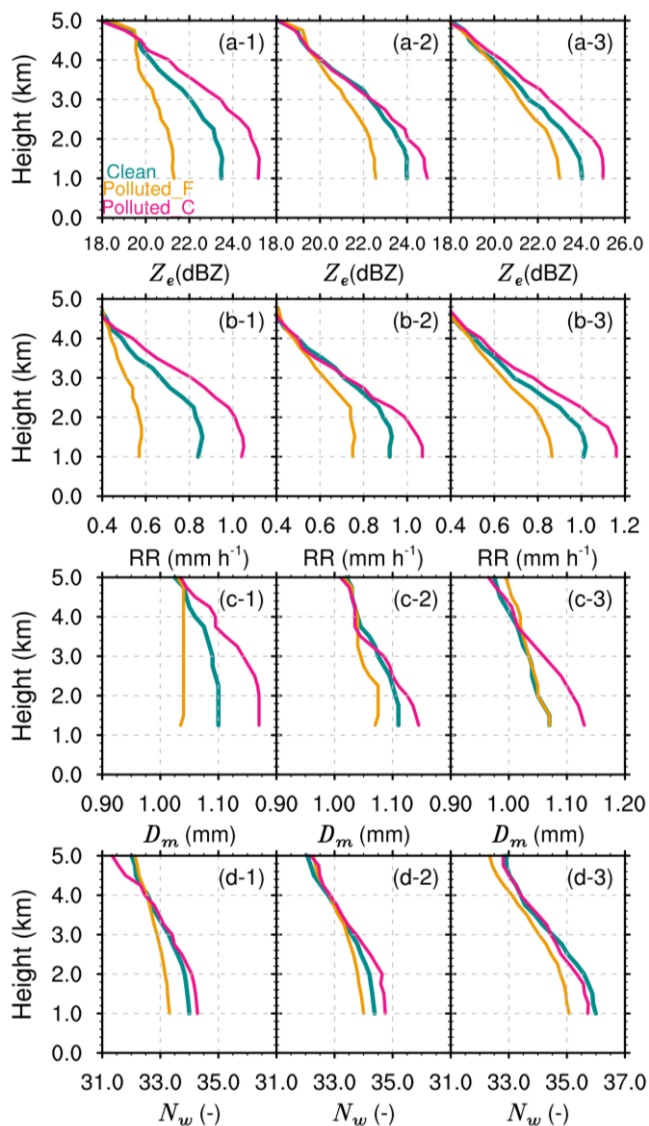
510 2014 to 2021. CAPE1, CAPE2, and CAPE3 are shown in the left, middle, and right
511 panels, respectively.

512

513 Similarly, the profiles of Z_e , RR, D_m , and N_w in different 850hPa-RH and aerosol
514 backgrounds are illustrated in Figure 9. Consistent with previous research results, the
515 median values of Z_e , RR, D_m , and N_w of shallow precipitation exhibit a gradual increase
516 with decreasing altitude, reflecting the warm rain collision-coalescence growth process.
517 However, the microphysical structures of shallow precipitation vary under different RH
518 conditions with similar aerosol backgrounds. As RH at 850hPa increases, the median
519 values of Z_e , RR, D_m , and N_w of shallow precipitation increase more significantly with
520 decreasing altitude. For example, under low humidity conditions (RH1), the median D_m
521 increases slightly when hydrometeors fall from 3 km to 1 km (Figure 9c-1), and even
522 decreases under fine aerosol-polluted conditions, indicating more breakup processes.
523 Subsequently, with increasing humidity, the increase in D_m becomes more apparent
524 (Figure 9c-3). For example, the median D_m increases from 1.05 mm to 1.15 mm in
525 coarse aerosol-polluted environments.

526 The median values of Z_e and RR across various aerosol backgrounds are markedly
527 elevated in environments contaminated with coarse aerosols across all altitude layers,
528 demonstrating a notable increase with decreasing altitude. Conversely, in conditions
529 contaminated by fine aerosols, the median values of Z_e and RR are at their lowest at
530 each altitude layer, exhibiting minimal increases as altitude decreases. This is consistent
531 with previous conclusions (Figures 4 and 8), further indicating that the impact of coarse
532 and fine aerosols on the near-surface RR and the precipitation structure is not sensitive
533 to dynamic and moisture conditions. However, from a microphysical structure
534 perspective, there are still some differences in aerosol backgrounds. Under low and
535 moderate humidity conditions (RH1 and RH2), at a given altitude, D_m and N_w are the
536 largest in coarse aerosol-polluted environments and the smallest in fine aerosol-polluted
537 environments. In RH3 conditions at the same altitude, a clean environment has the
538 highest N_w and a relatively small D_m ; for coarse mode, N_w is moderate with the largest
539 D_m ; and for fine mode, N_w is the lowest with a relatively small D_m . This indicates that
540 in high RH environments, fine aerosols mainly reduce RR by suppressing the
541 concentration of raindrops, while coarse aerosols increase RR by increasing the size of
542 hydrometeors. Furthermore, the differences in precipitation structures in aerosol-
543 polluted coarse and fine environments depend on humidity conditions, consistent with

544 the conclusions in Figure 7. The differences are the greatest under RH1 conditions, with
 545 the differences in RR, Z_e , D_m , and N_w at 1 km altitude being 0.42 mm h⁻¹, 4.5 dBZ, 0.19
 546 mm, and about 1.3, respectively. Under RH3 conditions, the differences are smallest,
 547 with the differences in the aforementioned variables being 0.35 mm h⁻¹, 2 dBZ, 0.05
 548 mm, and approximately 0.8, respectively.



549

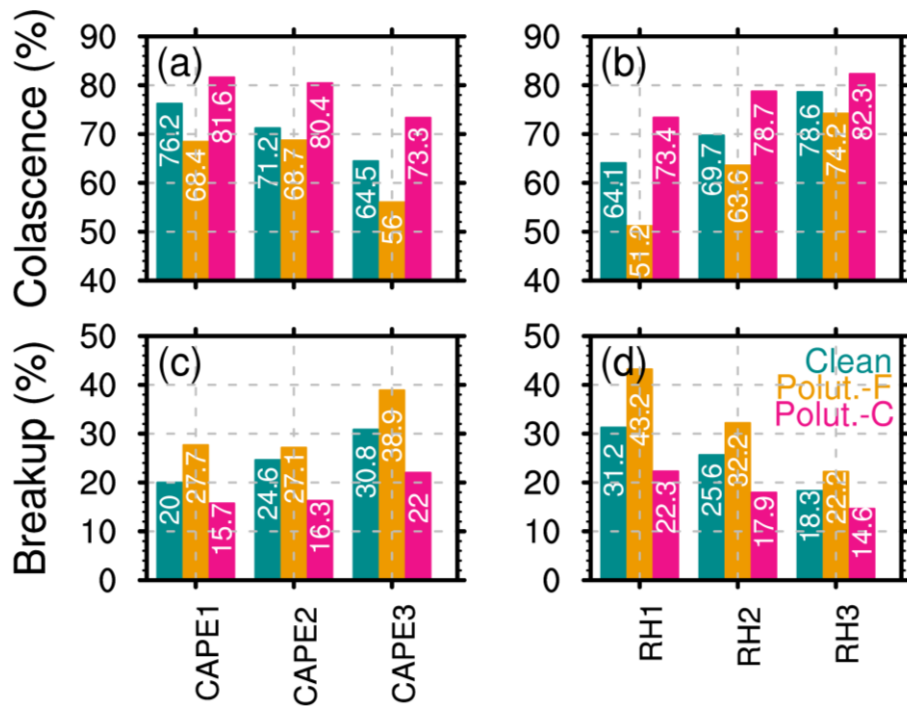
550 **Figure 9** The Z_e (a), rain rate (b), D_m (c), and N_w (d) profiles for shallow precipitation
 551 in different aerosol conditions and 850 hPa-RH over southern China during the
 552 summers from 2014 to 2021. RH1, RH2, and RH3 are shown in left, middle, and right
 553 panels, respectively.

554

555 To quantitatively analyze the dependence of microphysical processes on dynamics
556 and moisture under different aerosol backgrounds, we examined the differences in the
557 two primary microphysical processes, i.e., collision-coalescence and breakup. As a
558 result of the low proportions of size sorting and balance, further analysis of these
559 microphysical processes is not included. The microphysical processes of precipitation
560 depend on the dynamic and moisture conditions. For instance, with decreasing CAPE
561 and increasing RH, the proportion of collision-coalescence increases, while the
562 proportion of breakup decreases in clean, coarse, and fine aerosol-polluted
563 environments. Environments with high RH and low CAPE encourage aerosol particles
564 in the boundary layer to gather moisture, leading to the formation of additional cloud
565 droplets. These droplets then condense further to create more raindrops, thus enhancing
566 the collision-coalescence process.

567 After comparing various aerosol backgrounds, it is possible to determine certain
568 overarching patterns that remain consistent regardless of thermodynamic conditions.
569 Initially, irrespective of CAPE, RH, or aerosol background, shallow precipitation
570 systems predominantly exhibit the warm rain collision-coalescence process, with its
571 occurrence proportion spanning from a minimum of 51.2% to a maximum of
572 82.3%. There is also a certain proportion of break-up processes, ranging from 14.6% to
573 43.2%. Second, regardless of the value of CAPE and RH, the proportion of the
574 collision-coalescence process is always the highest in coarse aerosol-polluted
575 environments, while the proportion of the breakup process is always the highest in fine
576 aerosol-polluted environments. These conclusions are consistent with the results in
577 Figure 5. However, the increase in the proportion of collision coalescence in coarse
578 aerosol-polluted environments and the increase in the proportion of breakup in fine
579 aerosol-polluted environments depend on dynamic and moisture conditions. For
580 example, under low relative humidity (RH1) conditions, the proportion of the collision-
581 coalescence process in coarse aerosol-polluted environments (73.4%) is significantly
582 higher than that in fine aerosol-polluted environments (51.2%), with an enhancement
583 of 22.2%. On the contrary, the proportion of the breakup process in fine aerosol-
584 polluted environments (43.2%) is significantly higher than in coarse aerosol-polluted
585 environments (22.3%). This is consistent with previous findings that under RH1
586 conditions, D_m in fine aerosol-polluted environments rapidly decreases with decreasing
587 altitude.

588



589
 590 **Figure 10** The percentages of coalescence (a), size sorting (b), break-up(c), and balance
 591 (d) for shallow precipitation rain hydrometeors under different aerosol conditions in
 592 southern China during the summers from 2014 to 2021.

593 **4 Conclusion and Discussion**

594 Using the combined data of DPR, MERRA-2 aerosol datasets, and ERA5 during
 595 the summers of 2014-2021, this study investigates the potential impacts of coarse and
 596 fine aerosol modes on the Rain Rate (RR), microphysical structure, and processes for
 597 shallow precipitation in South China. Clean, coarse, and fine aerosol-polluted modes
 598 are classified according to the AOD for total aerosols, coarse aerosols, and fine aerosols
 599 derived from MERRA-2 products. ERA5 reanalysis data are used to explore the
 600 sensitivity of aerosol impacts on shallow precipitation to dynamic and moisture
 601 conditions in South China. The main findings are summarized as follows.

602 In comparison to clean environments, coarse aerosol-polluted environments
 603 enhance near-surface rainfall rates of shallow precipitation, characterized by stronger
 604 near-surface RR (average precipitation intensity of 1.78 mm h^{-1}), higher concentrations

605 (average $N_w = 36.98$) and larger raindrop sizes (average $D_m = 1.24$ mm) of hydrometeor
606 particles. This can be ascribed to the high presence of sea salt aerosols in South China,
607 which tend to form larger cloud droplets through hygroscopic growth, leading to larger
608 raindrop particles through microphysical processes such as condensation. On the
609 contrary, fine aerosol mode suppress near-surface RR, with an average near-surface RR
610 of only 1.33 mm h^{-1} and lower concentrations and smaller sizes of hydrometeors
611 (average $N_w = 36.37$, average $D_m = 1.14$ mm). Liu et al. (2022) noted similar opposing
612 effects of fine aerosols and coarse sea spray on warm marine clouds. Deep clouds show
613 increased rainfall with high liquid water content but reduced rainfall if water content is
614 low (Li et al., 2011). This underscores the distinct behavior of shallow precipitation and
615 the varied impacts of aerosol types on it. However, fine aerosol-polluted environments
616 promote vertical development of shallow precipitation clouds (median STH of 3.7 km),
617 approximately 0.5 km higher than in coarse aerosol-polluted conditions. The inhibition
618 of the vertical development of precipitation clouds by coarse aerosol particles explains
619 their suppressive effect on lightning activity to some extent (Pan et al., 2022).

620 From the perspective of precipitation vertical structure and microphysical
621 processes, shallow precipitation is dominated by warm-rain collision-coalescence
622 processes under different aerosol backgrounds, with the collision-coalescence process
623 accounting for over 62%. However, there are significant differences in the efficiency
624 of hydrometeor collision-coalescence growth under different aerosol conditions. In
625 contrast to clean conditions, the median values of Z_e , RR, D_m , and N_w are highest in
626 presence of aerosol coarse mode and lowest in conditions for fine aerosol mode at all
627 altitude levels. Looking at it from a microphysical standpoint, the increase in D_m with
628 decreasing altitude is most pronounced under coarse aerosol-polluted conditions,
629 reflecting more significant collision-coalescence growth processes, accounting for
630 74.1%. In contrast, the increase in D_m with decreasing altitude is weakest under fine
631 aerosol-polluted conditions, due to the higher proportion of breakup processes
632 (accounting for 33.1%) and a decrease of approximately 12% in the collision-
633 coalescence process (accounting for 62.4%). Overall, the promotion of RR is associated
634 with more significant collision-coalescence processes by coarse aerosols, while the

635 suppression of RR is characterized by more significant breakup processes with fine
636 aerosols.

637 The effects of fine and coarse aerosols on the suppression and enhancement of RR
638 are independent of CAPE and humidity, consistent with the findings by Liu et al. (2022).
639 However, our results show that the extent of suppression or enhancement varies with
640 CAPE and humidity. Additionally, the analysis of aerosol-precipitation interactions
641 under different surface air temperatures yields results similar to those observed for
642 CAPE and RH at 850 hPa (figures not shown). The promotion and suppression effects
643 are the most pronounced under low relative humidity conditions (RH1). This is mainly
644 contributed by the stronger suppression of fine aerosols in low-humidity environments.
645 For instance, the median RR is around 1.12 mm h⁻¹ under coarse aerosol-polluted
646 conditions, while it is around 0.7 mm h⁻¹ under fine aerosol-polluted conditions, with a
647 difference of approximately 0.42 mm h⁻¹. The collision-coalescence and breakup
648 microphysical processes play an important role in these differences, with the collision-
649 coalescence accounting for 73.4% under coarse aerosol-polluted conditions, which is
650 22.2% higher than the 51.2% observed under fine aerosol-polluted conditions.
651 Correspondingly, the breakup microphysical processes account for 43.2% under fine
652 aerosol-polluted conditions, significantly higher than the 22.3% in coarse aerosol-
653 polluted conditions. Under high relative humidity conditions, fine aerosol-polluted
654 environments primarily reduce RR by inhibiting hydrometeor concentration (possibly
655 as a result of the evaporation effects of small cloud droplets), while coarse aerosols
656 invigorate RR by increasing the size of hydrometeor particles. Additionally, the
657 increase in RR above 3 km in coarse aerosol-polluted environments is mainly driven
658 by the high concentration of hydrometeors in low instability conditions, while by large
659 hydrometeors in high instability environments. It is important to note that precipitation
660 is a complex process influenced by multiple meteorological factors, including
661 instability, moisture, and temperature. Additionally, other factors such as wind vectors
662 and pressure may also affect the impact of aerosols on precipitation, which is worthy
663 of further study.

664 This study primarily elucidates the microphysical processes within shallow

665 precipitation systems under varying aerosol conditions. However, the methods and data
666 utilized have broad application potential. Future research could extend these
667 approaches to explore the relationship between deep convection or mixed-phase clouds
668 and aerosols. Such investigations could reveal the complex effects of aerosols on the
669 precipitation process and further enhance our scientific understanding of the physical
670 connections between aerosols and precipitation microphysics. However, it is important
671 to note that the spatial resolution of MERRA-2 and ERA5 is much coarser than that of
672 DPR. The interpolation methods employed in the present study may introduce errors
673 and may not fully capture the true conditions, making it challenging to accurately assess
674 fine-scale processes in aerosol-cloud interactions. Furthermore, MERRA-2 shows a
675 slight underestimation of approximately 0.1 compared to in-situ observations in South
676 China (Ou et al., 2022), probably due to the absence of nitrate aerosols in the MERRA-
677 2 dataset. Consequently, the fine aerosol-polluted environments examined in this study
678 may not fully capture conditions with high nitrate loading. There is an urgent need for
679 long-term observational data on aerosol concentrations with high spatiotemporal
680 resolution and accuracy to fully capture the samples of high aerosol loading and more
681 effectively capture fine-scale processes in aerosol-cloud interactions.

682

683 **Data availability**

684 The GPM DPR data provided by NASA Goddard Space Flight Center's Mesoscale
685 Atmospheric Processes Laboratory and Precipitation Processing System (PPS) can be
686 downloaded from <https://pmm.nasa.gov/dataaccess/downloads/gpm>. MERRA-2 data
687 can be downloaded from [https://gmao.gsfc.nasa.gov/reanalysis/MERRA-
688 2/data_access/](https://gmao.gsfc.nasa.gov/reanalysis/MERRA-2/data_access/). The ERA5 data can be downloaded from
689 <https://www.ecmef.int/en/forecasts/dataset/ecmwf-reanalysis-v5>. The ancillary digital
690 terrain data is from the National Geophysical Data Center (NGDC) (available online at
691 <http://www.ngdc.noaa.gov>, accessed in May 2023).

692

693 **Author contributions**

694 YY designed the manuscript and led the data analysis; FC performed the analysis
695 and wrote the manuscript draft; YL and LY collected the data; GL, LY, and SL
696 reviewed and edited the manuscript; SL helped with the data analysis.

697 **Declaration of competing interest**

698 The authors declare no competing interests.

699

700 **Acknowledgments**

701 The authors thank NASA Goddard Space Flight Center's Mesoscale Atmospheric
702 Processes Laboratory and PPS, NGDC, and ECMWF for providing the analysis data.

703 **Financial support**

704 This work has been jointly supported by the China National Natural Science
705 Foundation (grant 42222503), the Jiangsu Meteorological Bureau General Project
706 (KM202407), the Open Grants of China Meteorological Administration Radar
707 Meteorology Key Laboratory (2024LRM-B06), the Open Project of KLME & CIC-
708 FEMD (KLME202303), China Meteorological Administration "Application of
709 quantum technology in meteorological detection" Youth Innovation Team Project
710 (No.CMA2024QN11), and the Open Project of State Key Laboratory of Severe
711 Weather (2024LASW-B11).

712

713

Reference

714

715 Buchard, V., da Silva, A. M., Colarco, P. R., Darmenov, A., Randles, C. A., Govindaraju, R., Torres, O.,
716 Campbell, J., and Spurr, R.: Using the OMI aerosol index and absorption aerosol optical depth to
717 evaluate the NASA MERRA Aerosol Reanalysis, *Atmos. Chem. Phys.*, 15, 5743-5760,
718 10.5194/acp-15-5743-2015, 2015.

719 Buchard, V., Randles, C. A., da Silva, A. M., Darmenov, A., Colarco, P. R., Govindaraju, R., Ferrare,

720 R., Hair, J., Beyersdorf, A. J., Ziemba, L. D., and Yu, H.: The MERRA-2 Aerosol Reanalysis,
721 1980 Onward. Part II: Evaluation and Case Studies, *Journal of Climate*, 30, 6851-6872,
722 <https://doi.org/10.1175/JCLI-D-16-0613.1>, 2017.

723 Chen, F., Zheng, X., Wen, H., and Yuan, Y.: Microphysics of Convective and Stratiform Precipitation
724 during the Summer Monsoon Season over the Yangtze–Huaihe River Valley, China, *Journal of*
725 *Hydrometeorology*, 23, 239-252, 2022.

726 Chen, F., Zheng, X., Yu, L., Wen, H., and Liu, Y.: Precipitation, microphysical and environmental
727 characteristics for shallow and deep clouds over Yangtze-Huaihe River Basin, *Atmospheric*
728 *Research*, 298, 107155, <https://doi.org/10.1016/j.atmosres.2023.107155>, 2024.

729 Chen, Y., Zhang, A., Zhang, Y., Cui, C., Wan, R., Wang, B., and Fu, Y.: A Heavy Precipitation Event in
730 the Yangtze River Basin Led by an Eastward Moving Tibetan Plateau Cloud System in the
731 Summer of 2016, *Journal of Geophysical Research: Atmospheres*, 125, e2020JD032429,
732 <https://doi.org/10.1029/2020JD032429>, 2020.

733 Chin, M., Ginoux, P., Kinne, S., Torres, O., Holben, B. N., Duncan, B. N., Martin, R. V., Logan, J. A.,
734 Higurashi, A., and Nakajima, T.: Tropospheric Aerosol Optical Thickness from the GOCART
735 Model and Comparisons with Satellite and Sun Photometer Measurements, *Journal of the*
736 *Atmospheric Sciences*, 59, 461-483, [https://doi.org/10.1175/1520-0469\(2002\)059<0461:TAOTFT>2.0.CO;2](https://doi.org/10.1175/1520-0469(2002)059<0461:TAOTFT>2.0.CO;2), 2002.

738 Christensen, M. W. and Stephens, G. L.: Microphysical and macrophysical responses of marine
739 stratocumulus polluted by underlying ships: 2. Impacts of haze on precipitating clouds, *Journal of*
740 *Geophysical Research: Atmospheres*, 117, <https://doi.org/10.1029/2011JD017125>, 2012.

741 Fan, C., Wang, M., Rosenfeld, D., Zhu, Y., Liu, J., and Chen, B.: Strong Precipitation Suppression by
742 Aerosols in Marine Low Clouds, *Geophysical Research Letters*, 47, e2019GL086207,
743 <https://doi.org/10.1029/2019GL086207>, 2020.

744 Fan, J., Rosenfeld, D., Zhang, Y., Giangrande, S. E., Li, Z., Machado, L. A. T., Martin, S. T., Yang, Y.,
745 Wang, J., Artaxo, P., Barbosa, H. M. J., Braga, R. C., Comstock, J. M., Feng, Z., Gao, W., Gomes,
746 H. B., Mei, F., Pöhlker, C., Pöhlker, M. L., Pöschl, U., and de Souza, R. A. F.: Substantial
747 convection and precipitation enhancements by ultrafine aerosol particles, *Science*, 359, 411-418,
748 [10.1126/science.aan8461](https://doi.org/10.1126/science.aan8461), 2018.

749 Gelaro, R., McCarty, W., Suárez, M. J., Todling, R., Molod, A., Takacs, L., Randles, C. A., Darmenov,
750 A., Bosilovich, M. G., Reichle, R., Wargan, K., Coy, L., Cullather, R., Draper, C., Akella, S.,
751 Buchard, V., Conaty, A., da Silva, A. M., Gu, W., Kim, G.-K., Koster, R., Lucchesi, R., Merkova,
752 D., Nielsen, J. E., Partyka, G., Pawson, S., Putman, W., Rienecker, M., Schubert, S. D.,
753 Sienkiewicz, M., and Zhao, B.: The Modern-Era Retrospective Analysis for Research and
754 Applications, Version 2 (MERRA-2), *Journal of Climate*, 30, 5419-5454,
755 <https://doi.org/10.1175/JCLI-D-16-0758.1>, 2017.

756 Guo, J., Su, T., Chen, D., Wang, J., Li, Z., Lv, Y., Guo, X., Liu, H., Cribb, M., and Zhai, P.: Declining
757 Summertime Local-Scale Precipitation Frequency Over China and the United States, 1981–2012:
758 The Disparate Roles of Aerosols, *Geophysical Research Letters*, 46, 13281-13289,
759 <https://doi.org/10.1029/2019GL085442>, 2019.

760 Huang, H., Zhao, K., Fu, P., Chen, H., Chen, G., and Zhang, Y.: Validation of Precipitation
761 Measurements From the Dual-Frequency Precipitation Radar Onboard the GPM Core Observatory
762 Using a Polarimetric Radar in South China, *IEEE Transactions on Geoscience and Remote*
763 *Sensing*, 1-16, [10.1109/TGRS.2021.3118601](https://doi.org/10.1109/TGRS.2021.3118601), 2021.

764 Iguchi, T., Seto, S., Meneghini, R., Yoshida, N., Awaka, J., and Kubota, T.: GPM/DPR level-2
765 algorithm theoretical basis document, NASA Goddard Space Flight Center, Greenbelt, MD, USA,
766 Tech. Rep, 2017.

767 Jiang, M., Li, Z., Wan, B., and Cribb, M.: Impact of aerosols on precipitation from deep convective
768 clouds in eastern China, *Journal of Geophysical Research: Atmospheres*, 121, 9607-9620,
769 <https://doi.org/10.1002/2015JD024246>, 2016.

770 Koren, I., Dagan, G., and Altaratz, O.: From aerosol-limited to invigoration of warm convective clouds,
771 *Science*, 344, 1143-1146, doi:10.1126/science.1252595, 2014.

772 Kumjian, M. R., Khain, A. P., Benmoshe, N., Ilotoviz, E., Ryzhkov, A. V., and Phillips, V. T. J.: The
773 Anatomy and Physics of ZDR Columns: Investigating a Polarimetric Radar Signature with a
774 Spectral Bin Microphysical Model, *Journal of Applied Meteorology and Climatology*, 53, 1820-
775 1843, 10.1175/JAMC-D-13-0354.1, 2014.

776 Lang, F., Huang, Y., Protat, A., Truong, S. C. H., Siems, S. T., and Manton, M. J.: Shallow Convection
777 and Precipitation Over the Southern Ocean: A Case Study During the CAPRICORN 2016 Field
778 Campaign, *Journal of Geophysical Research: Atmospheres*, 126, e2020JD034088,
779 <https://doi.org/10.1029/2020JD034088>, 2021.

780 Li, Z., Niu, F., Fan, J., Liu, Y., Rosenfeld, D., and Ding, Y.: Long-term impacts of aerosols on the
781 vertical development of clouds and precipitation, *Nature Geoscience*, 4, 888-894,
782 10.1038/ngeo1313, 2011.

783 Liu, C. and Zipser, E.: Regional variation of morphology of organized convection in the tropics and
784 subtropics, *Journal of Geophysical Research: Atmospheres*, 118, 453-466,
785 <https://doi.org/10.1029/2012JD018409>, 2013.

786 Liu, F., Mao, F., Rosenfeld, D., Pan, Z., Zang, L., Zhu, Y., Yin, J., and Gong, W.: Opposing comparable
787 large effects of fine aerosols and coarse sea spray on marine warm clouds, *Communications Earth
788 & Environment*, 3, 232, 10.1038/s43247-022-00562-y, 2022.

789 Lolli, S., Sicard, M., Amato, F., Comeron, A., Gil-Diaz, C., Landi, T. C., Munoz-Porcar, C., Oliveira,
790 D., Dios Otin, F., Rocadenbosch, F., Rodriguez-Gomez, A., Alastuey, A., Querol, X., and Reche,
791 C.: Climatological assessment of the vertically resolved optical and microphysical aerosol
792 properties by lidar measurements, sunphotometer, and in-situ observations over 17 years at UPC
793 Barcelona, *EGUsphere*, 2023, 1-29, 10.5194/egusphere-2023-893, 2023.

794 Miltenberger, A. K., Field, P. R., Hill, A. A., Rosenberg, P., Shipway, B. J., Wilkinson, J. M., Scovell,
795 R., and Blyth, A. M.: Aerosol–cloud interactions in mixed-phase convective clouds – Part 1:
796 Aerosol perturbations, *Atmos. Chem. Phys.*, 18, 3119-3145, 10.5194/acp-18-3119-2018, 2018.

797 Molod, A., Takacs, L., Suarez, M., and Bacmeister, J.: Development of the GEOS-5 atmospheric
798 general circulation model: evolution from MERRA to MERRA2, *Geosci. Model Dev.*, 8, 1339-
799 1356, 10.5194/gmd-8-1339-2015, 2015.

800 Ou, Y., Li, Z., Chen, C., Zhang, Y., Li, K., Shi, Z., Dong, J., Xu, H., Peng, Z., Xie, Y., and Luo, J.:
801 Evaluation of MERRA-2 Aerosol Optical and Component Properties over China Using SONET
802 and PARASOL/GRASP Data, *Remote Sensing*, 14, 821, 2022.

803 Pan, Z., Mao, F., Rosenfeld, D., Zhu, Y., Zang, L., Lu, X., Thornton, J. A., Holzworth, R. H., Yin, J.,
804 Efraim, A., and Gong, W.: Coarse sea spray inhibits lightning, *Nat Commun*, 13, 4289,
805 10.1038/s41467-022-31714-5, 2022.

806 Radhakrishna, B., Satheesh, S., Narayana Rao, T., Saikranthi, K., and Sunilkumar, K.: Assessment of
807 DSDs of GPM-DPR with ground-based disdrometer at seasonal scale over Gadanki, India, *Journal*

808 of Geophysical Research: Atmospheres, 121, 2016.

809 Randles, C. A., Da Silva, A. M., Buchard, V., Colarco, P. R., Darmenov, A., Govindaraju, R., Smirnov,
810 A., Holben, B., Ferrare, R., Hair, J., Shinozuka, Y., and Flynn, C. J.: The MERRA-2 Aerosol
811 Reanalysis, 1980 - onward, Part I: System Description and Data Assimilation Evaluation, *J Clim*,
812 30, 6823-6850, [10.1175/jcli-d-16-0609.1](https://doi.org/10.1175/jcli-d-16-0609.1), 2017.

813 Rosenfeld, D., Lohmann, U., Raga, G. B., O'Dowd, C. D., Kulmala, M., Fuzzi, S., Reissell, A., and
814 Andreae, M. O.: Flood or Drought: How Do Aerosols Affect Precipitation?, *Science*, 321, 1309-
815 1313, [10.1126/science.1160606](https://doi.org/10.1126/science.1160606), 2008.

816 Smalley, K. M. and Rapp, A. D.: The Role of Cloud Size and Environmental Moisture in Shallow
817 Cumulus Precipitation, *Journal of Applied Meteorology and Climatology*, 59, 535-550,
818 <https://doi.org/10.1175/JAMC-D-19-0145.1>, 2020.

819 Sun, E., Xu, X., Che, H., Tang, Z., Gui, K., An, L., Lu, C., and Shi, G.: Variation in MERRA-2 aerosol
820 optical depth and absorption aerosol optical depth over China from 1980 to 2017, *Journal of*
821 *Atmospheric and Solar-Terrestrial Physics*, 186, 8-19, <https://doi.org/10.1016/j.jastp.2019.01.019>,
822 2019a.

823 Sun, E., Che, H., Xu, X., Wang, Z., Lu, C., Gui, K., Zhao, H., Zheng, Y., Wang, Y., Wang, H., Sun, T.,
824 Liang, Y., Li, X., Sheng, Z., An, L., Zhang, X., and Shi, G.: Variation in MERRA-2 aerosol optical
825 depth over the Yangtze River Delta from 1980 to 2016, *Theoretical and Applied Climatology*, 136,
826 363-375, 2019b.

827 Sun, N., Fu, Y., Zhong, L., and Li, R.: Aerosol effects on the vertical structure of precipitation in East
828 China, *npj Climate and Atmospheric Science*, 5, 60, [10.1038/s41612-022-00284-0](https://doi.org/10.1038/s41612-022-00284-0), 2022.

829 Sun, Y. and Zhao, C.: Distinct impacts on precipitation by aerosol radiative effect over three different
830 megacity regions of eastern China, *Atmos. Chem. Phys.*, 21, 16555-16574, [10.5194/acp-21-](https://doi.org/10.5194/acp-21-16555-2021)
831 [16555-2021](https://doi.org/10.5194/acp-21-16555-2021), 2021.

832 Wang, M., Zhao, K., Xue, M., Zhang, G., Liu, S., Wen, L., and Chen, G.: Precipitation microphysics
833 characteristics of a Typhoon Matmo (2014) rainband after landfall over eastern China based on
834 polarimetric radar observations, *Journal of Geophysical Research: Atmospheres*, 121, 2016.

835 Xiao, Z., Zhu, S., Miao, Y., Yu, Y., and Che, H.: On the relationship between convective precipitation
836 and aerosol pollution in North China Plain during autumn and winter, *Atmospheric Research*, 271,
837 [106120](https://doi.org/10.1016/j.atmosres.2022.106120), <https://doi.org/10.1016/j.atmosres.2022.106120>, 2022.

838 Yang, Y., Wang, R., Chen, F., Liu, C., Bi, X., and Huang, M.: Synoptic weather patterns modulate the
839 frequency, type and vertical structure of summer precipitation over Eastern China: A perspective
840 from GPM observations, *Atmospheric Research*, 249, 105342,
841 <https://doi.org/10.1016/j.atmosres.2020.105342>, 2021.

842 Yuan, T., Remer, L. A., Pickering, K. E., and Yu, H.: Observational evidence of aerosol enhancement of
843 lightning activity and convective invigoration, *Geophysical Research Letters*, 38,
844 <https://doi.org/10.1029/2010GL046052>, 2011.

845 Zhang, A., Chen, Y., Zhang, X., Zhang, Q., and Fu, Y.: Structure of Cyclonic Precipitation in the
846 Northern Pacific Storm Track Measured by GPM DPR, *Journal of Hydrometeorology*, 21, 227-
847 240, <https://doi.org/10.1175/JHM-D-19-0161.1>, 2020a.

848 Zhang, Y., Yu, F., Luo, G., Chen, J.-P., and Chou, C. C. K.: Impact of Mineral Dust on Summertime
849 Precipitation Over the Taiwan Region, *Journal of Geophysical Research: Atmospheres*, 125,
850 [e2020JD033120](https://doi.org/10.1029/2020JD033120), <https://doi.org/10.1029/2020JD033120>, 2020b.

851